Catalysts **2015**, *5*, 1352-1374; doi:10.3390/catal5031352

OPEN ACCESS

catalysts

ISSN 2073-4344

www.mdpi.com/journal/catalysts

Article

Iron Fischer-Tropsch Catalysts Prepared by Solvent-Deficient Precipitation (SDP): Effects of Washing, Promoter Addition Step, and Drying Temperature

Kyle M. Brunner [1], Baiyu Huang [2], Brian F. Woodfield [2] and William C. Hecker [1,*]

[1] Department of Chemical Engineering, Brigham Young University, Provo, UT, 84602, USA; E-Mail: kyle.brunner@gmail.com

[2] Department of Chemistry and Biochemistry, Brigham Young University, Provo, UT, 84602, USA; E-Mails: baiyu.huang@gmail.com (B.H.); brian_woodfield@byu.edu (B.F.W.)

* Author to whom correspondence should be addressed; E-Mail: hecker@byu.edu; Tel.: +1-801-422-6235.

Academic Editor: Keith Hohn

Received: 10 April 2015 / Accepted: 15 July 2015 / Published: 24 July 2015

Abstract: A novel, solvent-deficient precipitation (SDP) method for catalyst preparation in general and for preparation of iron FT catalysts in particular is reported. Eight catalysts using a 2^3 factorial design of experiments to identify the key preparation variables were prepared. The catalysts were characterized by electron microprobe, N_2 adsorption, TEM, XRD, and ICP. Results show that the morphology of the catalysts, *i.e.*, surface area, pore volume, pore size distribution, crystallite sizes, and promoter distribution are significantly influenced by (1) whether or not the precursor catalyst is washed, (2) the promoter addition step, and (3) the drying condition (temperature). Consequently, the activity, selectivity, and stability of the catalysts determined from fixed-bed testing are also affected by these three variables. Unwashed catalysts prepared by a one-step method and dried at 100 °C produced the most active catalysts for FT synthesis. The catalysts of this study prepared by SDP compared favorably in activity, productivity, and stability with Fe FT catalysts reported in the literature. It is believed that this facile SDP approach has promise for development of future FT catalysts, and also offers a potential alternate route for the preparation of other catalysts for various other applications.

Keywords: Fischer-Tropsch synthesis; solvent-deficient precipitation; iron catalyst; catalyst preparation; catalyst characterization; Fischer-Tropsch catalyst

---

1. Introduction

Demand for liquid fuel sources combined with political unrest in some of the world's regions most abundant in oil and natural gas, in addition to the recent natural gas boom from hydraulic fracturing have pushed global and domestic energy policies to focus on domestic production and sustainability. This drive for domestic supplies of fuel provides opportunities for industrial innovation in developing and improving alternative liquid fuel sources, including natural gas, biomass, and coal. The Fischer-Tropsch synthesis (FTS) is one commercially proven process for producing hydrocarbon products from carbon monoxide and hydrogen (syngas) and is a key step in gas to liquid (GTL), biomass to liquid (BTL), and coal to liquid (CTL) technologies [1].

Catalyst preparation is a complex process intended to produce desirable chemical, physical, and catalytic properties in the final catalyst through choice of materials (*i.e*., metal, precursor, promoter, and support) and by manipulation of preparation variables and conditions (e.g., precipitation pH and temperature, washing, drying and calcination temperatures, and reduction environment and temperature) [2]. Promoters are added to catalysts to enhance their physical, chemical, and catalytic properties such as reduction temperature, rate of reaction, selectivity, or catalyst life. Supporting a catalyst on an oxide matrix (e.g., alumina, silica, ceria, or titania) requires extra preparation time and steps, but is desirable when the precursor is expensive (as is the case for cobalt or precious metal catalysts) or when structural enhancements (e.g., surface area, pore volume, or pore diameter) increase the dispersion, selectivity, or stability of the catalyst. Preparation variables largely determine the crystallite size, dispersion of the catalyst, and the pore and surface structure. After preparation, iron catalysts require pretreatment in order to create iron carbide, which is the active phase for FTS. Commercial iron FT catalysts at Sasol and at Synfuels China (currently the only commercial scale facilities using iron catalysts) are unsupported and precipitated catalysts promoted with copper or manganese (Synfuels China), potassium, and silica. This study focuses on catalysts promoted with copper, potassium and silica.

Good, extensive and detailed reviews of precipitated catalysts have been published [2,3]. A brief summary follows. Near the end of WWII and following, Ruhrchemie developed the first commercial iron catalyst which was used (and later modified) by Sasol [4]. Preparation involved pouring a near boiling solution of iron and copper nitrates (5 g Cu per 100 g Fe) into a hot solution of sodium carbonate while controlling pH around 6. After extensive washing in hot water to remove sodium, the precipitate was slurried and impregnated with potassium silicate (25 g SiO_2 per 100 g Fe) to improve thermal stability. Potassium was removed by adding nitric acid until the desired amount of potassium remained (5 g K per 100 g Fe). The effects of preparation method such as the precipitation order (acid into base or *vice versa*), final pH, temperature, viscosity of solvent at drying time, calcination temperature, and reduction temperature and environment (H_2 only or H_2 + CO) were known but not necessarily understood. Commercial catalysts used at Sasol and at Synfuels China are modifications of the Ruhrchemie catalyst. Although other methods and formulations have been developed, the fact that the Ruhrchemie preparation is still used in modified forms speaks to the robust nature and activity of these catalysts.

Improvements on the Ruhrchemie catalyst have been developed both by academic and industrial interests. Early work by Sasol showed: (1) lower required reduction temperature with increasing Cu content, (2) increased thermal stability and pore structure with increasing SiO_2 content, and (3) increased wax selectivity with increasing K content [4]. Later, Texas A&M studies spanning more than

10 years resulted in a continuous co-precipitation method to carefully control pH and temperature, resulting in highly active, selective, and stable catalysts for both FB and slurry reactor applications [5–8] which are among the most active iron catalysts reported in the literature to date [5–8]. Studies showed that K inhibits reducibility, increases WGS and iron FTS activity, and increases selectivity to olefins and heavy hydrocarbons. It was suggested that at higher K loadings, the apparent decrease in activity may be due to increased diffusion effects from pores filled with heavier molecular weight hydrocarbons. Increasing SiO_2 loading increased stability, but decreased reducibility, activity, and selectivity possibly due to diminishing effectiveness of Cu and K loadings as SiO_2 interacts with and neutralizes the effects of Cu and K. Cu increases reducibility and promotes WGS activity. Studies at UC Berkeley focused on promoter effects (K, Zn, Cu, and Ru) and on the effects of solvent viscosity on surface structure and promoter dispersion [9]. The goal was to increase the density of CO binding sites, thus bringing Fe catalysts to a level of activity comparable to that of Co catalysts. Promoters increased site density by encouraging smaller nucleation sites during reduction and reaction. Replacing water in precursor pores with low surface tension alcohols resulted in larger surface areas. Catalysts prepared by this method were of comparable activity to a low activity Co catalyst and had lower selectivities to CH_4. Work at the Chinese Academy of Science Institute of Coal Chemistry and by Synfuels China not only explored the effects of other metal promoters such as Mn but also produced highly active, stable and selective catalysts from sulfur-containing precursors which traditionally have been avoided due to the strong poisoning behavior of sulfur [10,11]. Recent studies showed that there could be an optimal range of K loading on Fe-based FTS catalysts, since higher K loading generally resulted in higher carburization rate, though too much K would lead to excessive carbon deposition [12,13].

Co-precipitation from aqueous solutions of precursors has been the principle preparation method for iron FT catalysts in the past; however, recent breakthroughs in solvent-deficient precipitation (SDP) of transition metal oxide nanoparticles by the BYU Chemistry Department and Cosmas Inc. provide exciting new possibilities for simpler, more uniform, and faster catalyst preparation methods [14–21]. Nanoparticle size distributions are tight and can be controlled over several orders of magnitude (1–10,000 nm) by simple factors such as adding water during the reaction, washing after reaction, and calcining at different temperatures. Successful synthesis of nanoparticle oxides has been achieved on over 20 different transition metals, rare earth metals, and groups I, II, and III of the periodic table including Ti [20], Al [16–18], Zr, Ni, Cu, Fe, Co, and La, all of which are common catalyst or support materials. To the best of our knowledge, the Cosmas SDP method had never been used for preparation of a catalyst prior to our current work. A report describing the preparation and performance of one Fe FT catalyst using the SDP method was published earlier this year [22]. It was also the subject of a dissertation [23].

In this paper, we report the preparation of eight iron FT catalysts and the use of a 2^3 factorial design of experiments to identify the key preparation variables. The catalysts are characterized by microprobe, N_2 adsorption, TEM, XRD, and ICP. Results show that the morphology of the catalysts, *i.e.*, surface area, pore volume, pore size distribution, crystallite sizes, and promoter distribution are significantly influenced by drying, washing, and the promoter addition step. Consequently, the activity, selectivity, and stability of the catalysts are also affected by these three variables. We also compare the catalysts in this study with other published, highly active iron FT catalysts. Results show that catalysts prepared via the SDP method have comparable or even better activity, productivity, and stability than traditional

Fe FT catalysts. Thus, this facile SDP approach seems to have potential for the development of not only FT catalysts, but also for preparing heterogeneous catalysts for other applications as well.

2. Results and Discussion

2.1. Catalyst Characterizations

2.1.1. Catalyst Nomenclature Description

To investigate the effects of three key preparation variables—(1) timing of the addition of promoters potassium and silica, (2) presence or absence of a washing step for the precursor, and (3) drying temperature—two levels of each of these variables were chosen. Each level is represented by a single alphanumeric character, as shown in Scheme 1. The eight catalysts of the factorial design are designated by the three characters representing the variable levels. Levels for timing of promoter addition were "1 Step" (designated by a 1) in which potassium and silica promoters were added to the salts of iron and copper before precipitation, and the catalyst was created in a single step, and "2 Step" (designated by a 2) in which potassium and silica promoters were added in a separate step after precipitation and washing, if applicable. The levels for washing were unwashed (U) or washed (W) using 100 mL of deionized water five times immediately following precipitation. Levels for initial drying temperature were high (H) temperature (100 °C) and low (L) temperature (60 °C overnight, followed by 100 °C). The six alphanumeric characters for catalyst designation represent the levels of the promoter addition (1 or 2), washing (U or W), and drying steps (L or H). For example, 1UH designates a catalyst prepared in 1 Step (with potassium and silica added to salts before precipitation), not washed (unwashed) after precipitation, and dried at the high drying temperature condition (100 °C). 2WL denotes a catalyst prepared in two steps (with potassium and silica added after precipitation and washing), washed directly after precipitation, and dried first at the low drying temperature (60 °C) followed by drying at 100 °C.

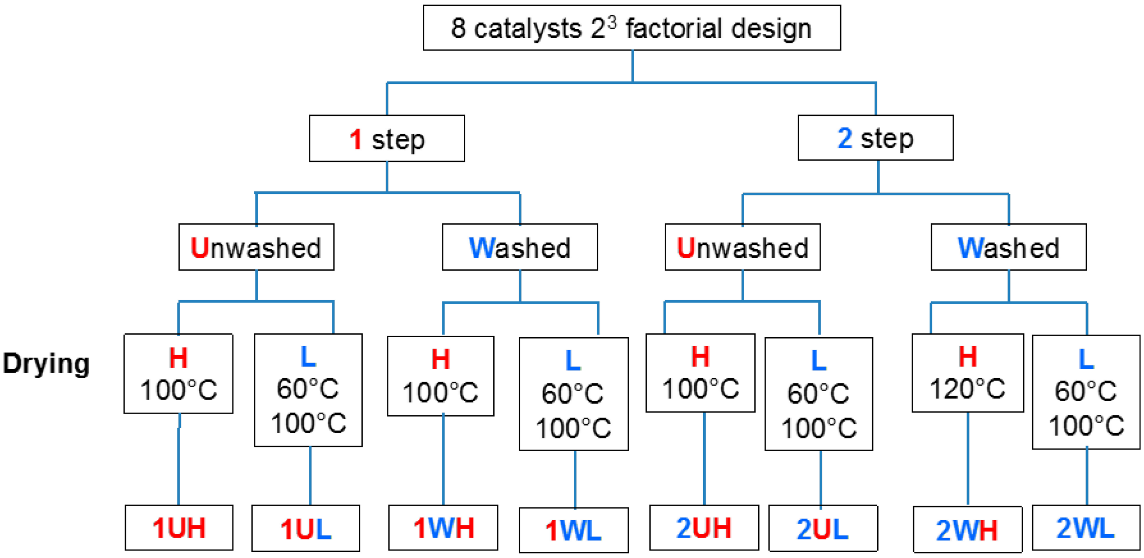

Scheme 1. 2^3 Factorial design for eight catalysts of this study.

2.1.2. Catalyst Compositions and Metal Distributions

Catalyst elemental compositions determined by ICP analysis are shown in Table 1 and are in good agreement with nominal compositions, except for the 1 Step washed catalysts (1WH, 1WL). ICP analysis of Si content in all cases was unreliable due to the formation of volatile SiF_4 during digestion and therefore are not reported.

Table 1. Compositions and pore properties of Fe catalysts.

Catalyst	**Nominal Composition (pbm)** [a]	**ICP composition** [b] **(pbm)**	**Fe Content** [c] **(Mass%)**	**Surface Area** [d] **(m^2/g)**	**Pore Volume** [e] **(cm^3/g)**	**Pore diameter (nm)**	**Pore Range** [f] **(nm)**
1UH	100Fe/5.0Cu/4.0K/16.0SiO_2	100Fe/5.1Cu/3.6K	66.3	45.6	0.14	10.3	6.3–17.4
1UL	100Fe/5.0Cu/4.0K/16.0SiO_2	100Fe/4.8Cu/3.7K	72.1	51.7	0.13	8.1	4.2–15.5
1WH	100Fe/5.0Cu/4.0K/16.0SiO_2	100Fe/4.9Cu/0.3K	62.1	55.6	0.24	15.5	8.7–28.0
1WL	100Fe/5.0Cu/4.0K/16.0SiO_2	100Fe/5.1Cu/0.3K	70.2	37.2	0.24	34.2	16.1-70.7
2UH	100Fe/5.0Cu/4.0K/16.0SiO_2	100Fe/4.1Cu/3.6K	68.0	36.8	0.14	8.7	5.0–15.3
2UL	100Fe/5.0Cu/4.0K/16.0SiO_2	100Fe/5.5Cu/4.2K	62.8	54.7	0.15	13.1	4.0–43.0
2WH	100Fe/5.0Cu/4.0K/16.0SiO_2	100Fe/5.3Cu/5.2K	65.1	65.7	0.13	5.5	1.2–12.8
2WL	100Fe/5.0Cu/4.2K/16.0SiO_2	100Fe/5.1Cu/5.0K	72.8	23.6	0.20	46.1	16.6–127.8

[a] parts by mass equal to g per 100 g_{Fe}; [b] SiO_2 not quantified by ICP; [c] after reduction and passivation; [d] 95% confidence interval = ±2.1 m^2/g; [e] 95% confidence interval = ±0.01 cm^3/g; [f] ±2 standard deviations of log normal pore diameter.

Figure 1 shows Fe, Cu, K, and SiO_2 distribution for 1UH, 2UH, and 2WH at the micron scale. Since Fe constitutes 60%–66% of these passivated catalysts, images of the other elements are compared to images of Fe to show contrasts in distributions. Figure 1a shows a microprobe image of a 50 μm agglomerate of 1UH. The distributions for Cu, K, and SiO_2 show uniform intensities and give the same details of cracks and boundaries as Fe. This indicates that the Cu, K, and Si distributions are uniform and that the promoters are in intimate association with Fe.

A similar 50 μm view of an agglomerate of 2UH (Figure 1b) shows a marked difference in elemental distributions of K and Si compared to 1UH. While Figure 1b shows uniform distributions of Fe and Cu, preferential distributions of K and Si along particle boundaries are observed. The center of the agglomerate shows almost no signal for K and Si, but since the signals lack sharp and well-defined edges, it appears that the promoters are distributed within outer structures and spaces and beginning to penetrate inward with the much smaller K^+ ions penetrating farther than the large clusters of SiO_2. This observation is supported by the fact that water was not added to 2UH during promoter addition as the precursor appeared moist enough to completely dissolve the $KHCO_3$ and SiO_2. The minimal amount of moisture distributed the promoters between particles, but the pores, already filled with a nearly saturated solution of NH_4NO_3 byproduct, presented some diffusional resistance for the promoters and prevented full penetration and uniform dispersion of the promoters.

A view of an agglomerate of 2WH at the same scale (Figure 1c) shows much better penetration of K and Si into the particles than Figure 1b. The K signal appears to reflect the structure shown by the Fe signal and shows no preferential accumulation at particle boundaries. The very center of the agglomerate shows some decrease, but not complete absence of signal. The Si signal clearly shows the structure and defects observed in the Fe distribution. The signal within the agglomerate is uniform despite the fact that the outside edges of the particle show well-defined edges and a stronger signal. Strong signal is also shown in spaces devoid of Fe signal between closely spaced particles. This is explained in part by the washing process and method of promoter addition. For 2WH, promoters were first dissolved in a minimal amount of water and then added to the precursor. Vacuum filtration following washing leaves the precursor relatively dry and the solution containing the promoters is readily absorbed into the pores, but there is still a tendency to accumulate on the outer edges of the particle, especially for SiO_2.

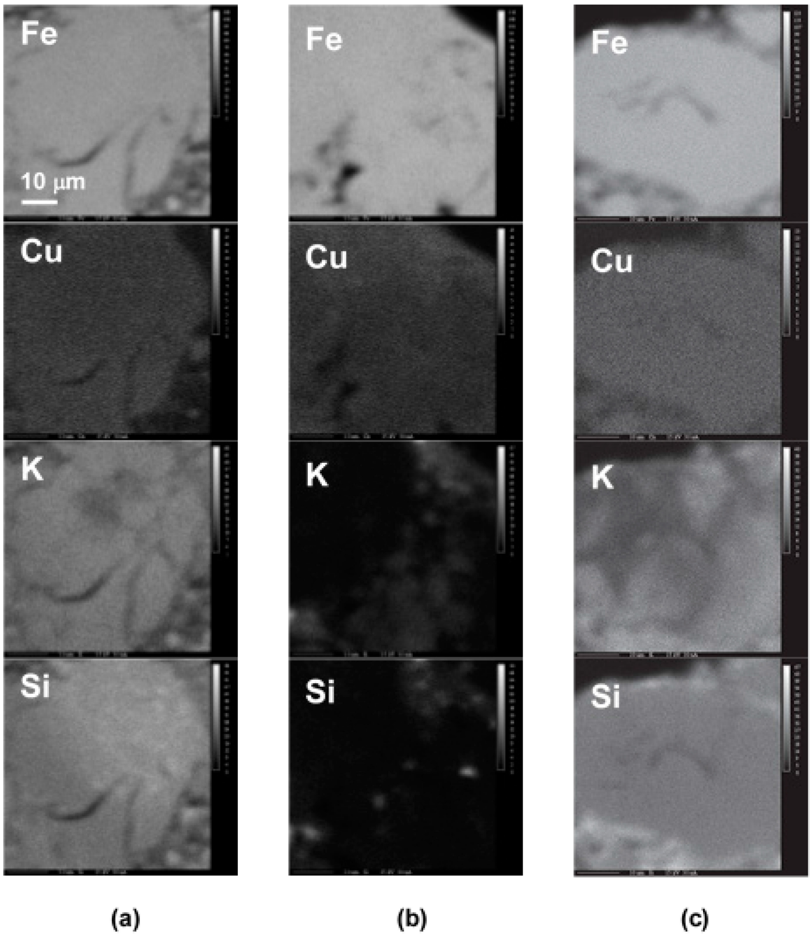

Figure 1. Electron microprobe images showing distributions of Fe, Cu, K, and Si of an agglomerate of (**a**) 1UH, (**b**) 2UH, and (**c**) 2WH.

From this analysis, it is clear that the promoters in 1S preparations are more uniformly distributed than in 2S preparations. While the byproduct is present in both 1UH and 2UH, the uniform distribution of potassium and silica promoters in 1UH shows that the promoters are intimately mixed with the Fe and their distribution is unaffected by diffusion through concentrated solutions of the byproduct as opposed to 2UH in which the diffusion hinders full penetration of particles by the promoters. Promoter distribution in 2WH is uniform within particles (despite higher concentrations on the outside edges of particles) due to removing the byproduct (by washing) and much of the water (by vacuum) so that the solution of promoters is readily absorbed into pores, whereas in 2UH the promoters are more concentrated near particle boundaries.

2.1.3. Catalyst Pore Structure and Crystallite Size

BET data for reduced and passivated catalysts are summarized in Table 1. Surface areas for the four 1S catalysts are 37.2–55.6 m^2/g, whereas surface areas for the four 2S catalysts are 23.6–65.7 m^2/g. For all catalysts, surface area follows the same order of progression with WL < UH < UL < WH. One study on the effect of SiO_2 loading on precipitated iron catalyst surface area reported catalysts with no SiO_2 having reduced surface areas of 10 m^2/g or less (after reduction in H_2), whereas catalysts with 8 or 24 parts SiO_2 per 100 parts Fe have surface areas of 98 m^2/g and 150 m^2/g (after reduction in CO), respectively [24]. If reduction in CO rather than H_2 gives larger surface areas by a factor of 2–3 as it appears to do, then the surface areas of 1S and 2S catalysts are between reported surface areas for precipitated catalysts containing 8 and 24 parts SiO_2, as expected. Notable exceptions are 2UH and 2WL, which have surface areas less than 40 m^2/g. These low surface area values support the previous supposition that the distribution of SiO_2 in these catalysts is not uniform.

Pore volumes of all reduced catalysts are 0.13–0.24 cm^3/g with washed catalysts giving larger pore volumes (0.13–0.24 cm^3/g compared with 0.13–0.15 cm^3/g) except 2WH (0.13 cm^3/g), which is a washed catalyst dried at 120 °C rather than 100 °C. The smaller pore volumes of the unwashed catalysts again suggest a different precursor structure than is found in the structure of the washed catalysts.

Pore diameters for the catalysts follow log-normal distributions with average pore diameters between 5.5 and 46.1 nm (see Table 1 and Figure 2). Figure 2a shows pore size distributions (PSD) for 1S catalysts. The pore size distributions for 1UH and 1UL are very similar at 4–200 nm, whereas the distributions for 1WH and 1WL are broader at 4–600 nm. Average diameters for 1UH and 1UL are 10.3 nm and 8.1 nm, respectively, whereas 1WH is 50–100% larger at 15.5 nm, and 1WL is 220–320% larger at 34.2 nm. Thus, for the 1S preparation, unwashed catalysts have smaller pores and narrower distributions of pores.

Further study of PSDs indicates that drying temperature has a combined effect with the presence of water such that lower drying temperatures correspond to larger pores (and larger particles). BET measurements on 1S catalysts were taken after calcination and again after reduction. 1S PSDs after calcination are nearly identical and show only pores smaller than 9 nm with averages between 2 nm and 4 nm; however, the PSDs after reduction are very different, as described above and shown in Figure 2a. Since all of the 1S catalyst pore structures are nearly identical after calcination, differences after reduction would not be expected. These differences after reduction could be due to the extent that the structures after drying lend themselves to particle growth (sintering) and to reduction, *i.e.* degree of crystallinity and contact between particles. It has been reported that the degree of crystallinity of ferrihydrite (precursor) increases as a function of temperature and time in the presence of water [25]. One theory of agglomeration states that linkages between molecules of water on the surfaces of smaller particles cause the particles to agglomerate. When the water is driven off, the ordered linkages lend themselves to phase transition from ferrihydrite to Fe_2O_3 as larger agglomerates [26]. Thus, pore size (which is related to particle size) increases with time and temperature in the presence of water. The lower drying temperature for 1WL may have driven water off slowly enough and provided enough time to increase the agglomeration sufficiently and create larger linked agglomerates which resulted in the largest pore size distribution of the 1S catalysts. The higher drying temperature of 1WH afforded the creation of some linkages (more so than in 1UH or 1UL, which had no water added), but drove the water off too quickly to create the extensive linking in the larger agglomerates of 1WL. Thus, the 1WH PSD is larger than 1UH and 1UL, but slightly smaller than 1WL.

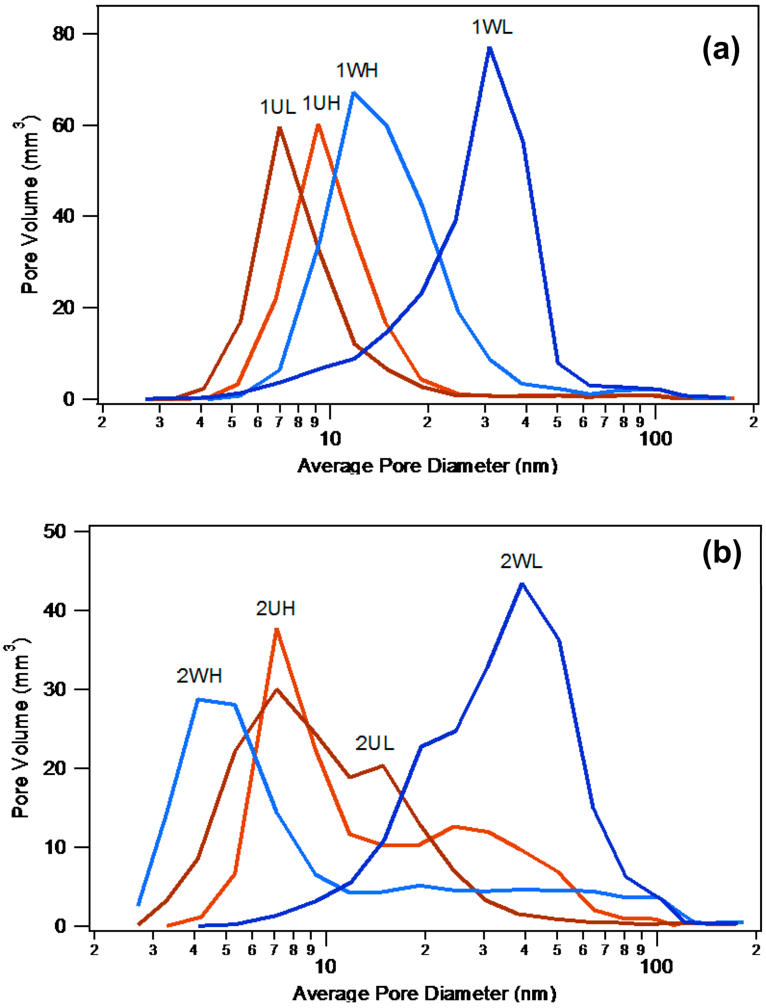

Figure 2. Pore size distributions of (**a**) 1S and (**b**) 2S catalysts after reduction and passivation.

Since the PSDs of 1UH and 1UL are very similar, it follows that drying temperature alone has very little effect on PSD. The reason may be that in these unwashed precursors, the formation of inter-particle linkages is inhibited. As shown in Equations 1 and 2 the products of reaction provide 10 molecules of H_2O for every atom of Fe in the preparation. This is more than adequate for hydration and coordination of the precursor, yet the PSDs of 1UH and 1UL are almost identical. Even though there is plenty of water present, the water is nearly saturated with byproduct NH_4NO_3. To the original agglomeration theory related above (see Figure 3), this work adds that the byproduct NH_4NO_3 may interfere with the weak water linkages between particles, making it difficult for larger agglomerates to form. Once dry, the particles are no longer free to form linkages and agglomerate, resulting in more narrow PSDs and smaller average diameters.

$$Fe(NO_3)_3\,9H_2O + 3NH_4HCO_3 \rightarrow Fe(OH)_3 + 3NH_4NO_3 + 9H_2O + 3CO_2 \quad (1)$$

$$Fe(OH)_3 \rightarrow FeOOH + H_2O \quad (2)$$

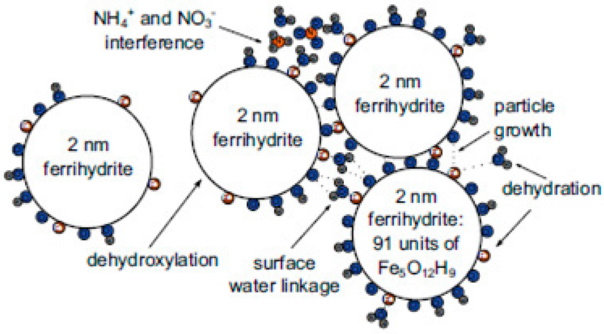

Figure 3. Illustration of agglomerate formation from ferrihydrite precursor particles. Large circles represent cross-sections of 2 nm spheres of ferrihydrite, whereas smaller circles represent 1.5 Å atomic cross-sections. Adapted from Ref. [24].

PSDs for the four 2S catalysts are shown in Figure 2b. The PSD for 2UH shows a bimodal distribution with the first average pore size at 8.7 nm and a +/−2σ range from 5.0 nm to 15.3 nm representing only 60.8% of the total pore volume as given in Table 1. The second average pore size at 34.6 nm has a +/−2σ range from 12.5 nm to 99.1 nm and accounts for 38.2% of the pore volume. The PSD for 2UL is fit as a single peak, even though it has a slight shoulder representing a second peak, giving a volume weighted average diameter of 13.1 nm and a range of 4.0–43.0 nm. The average pore diameter of 2WL is 46.1 nm and the range is 16.6–127.8 nm. It is interesting to note that PSDs for these three 2S catalysts cover much broader ranges of diameters than their 1S counter parts. 2WH is the exception and is discussed below. Like 1WL for 1S catalysts, 2WL has the largest average pore diameter and PSD of 2S catalysts. In contrast to the 1U catalysts, the PSDs for 2UH and 2UL are quite broad. The primary PSD for 2UH is in the expected narrow range and of smaller average diameter for an unwashed catalyst as explained above, but the secondary PSD is much larger. A comparison of PSDs of 2S catalysts after calcination with PSD after reduction indicates that this secondary range may be the result of adding precursors in a second step. The PSDs after calcination for all 2S catalysts have bimodal distributions with 50–75% of the pore volume in pores less than 9 nm. The balance of the pore volume for all of these catalysts spans the pore sizes described above. This shows that while the primary PSDs increased with reduction, the secondary PSDs for these catalysts did not. This behavior is expected if the secondary PSDs are filled with and supported by SiO_2 which was added in the second preparation step. For 2UL, to which more than an adequate amount of water was added during promoter addition, the extra water may have diluted the byproduct enough so that it did not interfere with the formation of linkages between particles leading to a larger PSD than 1UL and also to a larger PSD than the primary PSD of 2UH.

In contrast to the other three 2S catalysts, 2WH has smaller average pore diameters and narrower PSDs than all other catalysts. With other catalysts dried at the lower temperature, linkages formed between particles produced larger pore sizes and broad PSDs after reduction, but for catalysts dried at 120 °C, any linkages that may have formed appear to have been destroyed. This suggests that at 120 °C an energy barrier is surpassed which does more than simply dehydrate inter-particle linkages. One DSC/TGA study on ferrihydrite shows an endothermic transformation around 105–125 °C and also suggests that the surface of the ferrihydrite particles are covered in hydroxide groups [27]. Others show that drying at 130 °C results in partially dehydroxylating the ferrihydrite [28]. These two observations may be related, meaning that the endothermic transformation may actually be a removal of the surface hydroxides. A particle undergoing partial dehydroxylation would lose its surface hydroxides at temperatures lower than its interior hydroxides, leaving an oxide surface with a protected oxyhydroxide core. Surface hydroxides are the likely structures to form linkages with surface water between particles. As described above, slowly dehydrating the linked structures leads to larger agglomerates that grow into single particles of Fe_2O_3. At 120 °C, the water linkages may dehydrate at the same time that the surface hydroxides decompose which would destroy any linkages between particles and result in smaller pore diameters and very narrow PSDs.

Dispersion and average crystallite diameters of iron particles for all catalysts are listed in Table 2. Diameters estimated from chemisorption follow the trends for pore diameter and PSD and particle size is attributed to the agglomeration theory discussed above. Estimated average crystallite diameters for 1UH, 1UL, and 1WH agree amazingly well with their average pore diameters (within ±0.8 nm), while 1WL is within 5 nm (14%) of its average pore diameter (see Figure 4). Estimated diameters for 2UH, 2UL, and 2WL are roughly half of their pore diameters whereas the crystallite diameter for 2WH is within 1 nm (20%) of its pore diameter. Diameters from XRD data for Fe crystals in the passivated catalysts are larger than the diameters calculated from H_2 chemisorption. Diameters for Fe_3O_4 crystals are also larger than chemisorption diameters, except for 1WH, 1WL, 2UL, and 2WL.

Table 2. H_2 and CO uptakes, extents of reduction, dispersions, and crystallite diameters of catalysts after re-reduction in H_2 at 300 °C for 6 h.

	Uptake [a]					Crystallite diameter		
Catalyst	H_2 [b]	CO [c]	CO/H [d]	EOR	Disp	H_2 [a]	Fe [e]	Fe_3O_4 [e,f]
	μmol/g	μmol/g	%	%	nm	nm	nm	nm
1UH	159	583	1.85	21.5	12.5	9.8	19.7	20.5
1UL	146	893	3.05	15.5	14.8	8.3	19.8	22.6
1WH	203	746	1.85	46.1	8.0	15.3	26.3	15.2
1WL	131	675	2.60	50.6	4.2	29.5	36.4	21.2
2UH [g]	158	145	0.46	9.3	31.1	3.9	-	24.5
2UL	118	264	1.10	12.1	17.4	7.1	17.8	6.6
2WH	164	242	0.75	14.8	19.0	6.5	18.3	16.4
2WL	61	166	1.35	14.2	6.7	18.5	35.0	16.2

[a] after re-reduction for 6 h at 300 °C; [b] 95% confidence interval = ± 25%; [c] 95% confidence interval = ± 23%; [d] assume H concentration is double of H_2 concentration; [e] from XRD peak broadening; [f] Fe_3O_4 indistinguishable from FeO; [g] 2UH showed 26.8 nm Fe_2O_3, but no Fe.

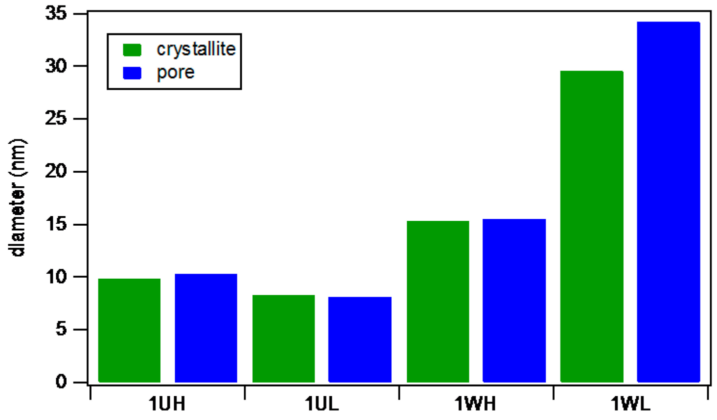

Figure 4. Comparison of average pore diameters from BET with average Fe crystallite diameters calculated from H_2 uptake for 1S catalysts.

TEM images of catalysts confirm the presence of crystallites with particle diameters equal to those estimated from chemisorption and XRD analysis. Figure 5 shows TEM images of 300 nm agglomerates of 1UH and 1WH, respectively. Figure 5a shows fine grains (5–10 nm) clumped together in 20–30 nm agglomerates, some of which have begun to merge into continuous particles, but which retain textures of the fine grains. This confirms the chemisorption crystallite diameter estimate of 9.8 nm for 1UH and also the 20 nm diameter XRD estimates of Fe and Fe_3O_4 crystals. The TEM image of 1WH (Figure 5b) shows much coarser single grains 10–30 nm in size. In contrast with 1UH, these larger particles appear to be continuous without smaller constituent pieces or textures. This also confirms the chemisorption diameter estimate of 15.3 nm as well as the XRD estimates of Fe (26.3 nm) and Fe_3O_4 (14.1 nm) crystallite diameters.

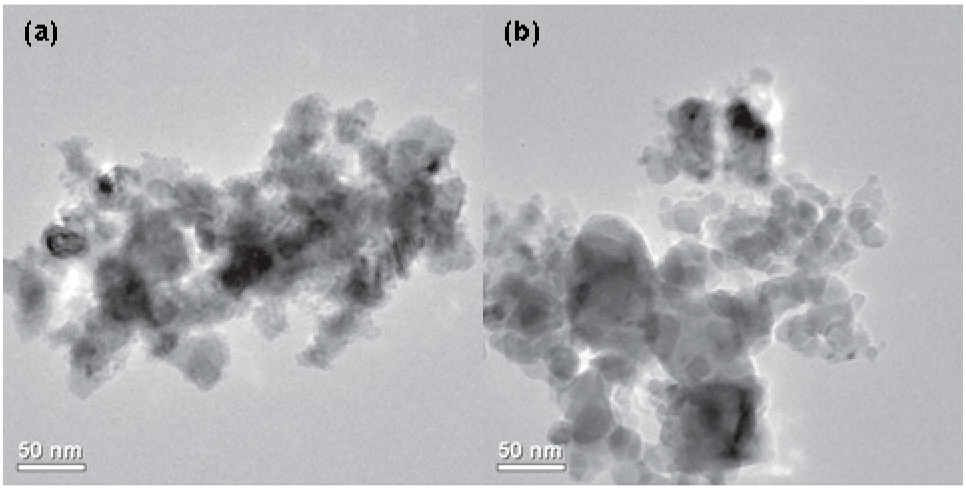

Figure 5. TEM micrograph of (**a**) 1UH and (**b**) 1WH catalysts.

2.2. Catalytic Performance

2.2.1 Catalyst Activity

Figure 6 shows experimental rate constant (*k*) values as functions of temperature for all the catalysts of this study. The solid lines were obtained using the Arrhenius equation and “best-fit” A and E_A values obtained from the k data for each catalyst. The most active catalyst is 2UH, followed by 1WL, 1UL, 1UH, and 2UL at 250 °C. Excluding 1WL and 1WH which have low K loadings, all 1U and 2U catalysts are more active than W catalysts at 250 °C. The activity for these catalysts may be explained by the iron carbide phase after reaction. As shown in Figure 7, the tallest and broadest peak for all catalysts (except 1WH) corresponds to Fe_2C, which may be a candidate for the active phase of the catalyst. 1UH, 1WL, 2UH, and 2UL (which are the most active catalysts) show the least signal (or none at all) for Fe_3O_4 and Fe_5C_2. 1UL, 1WH, 2WH and 2WL have strong Fe_5C_2 peaks, whereas 1UL and 1WH also show peaks for Fe_3O_4. As stated previously, these results do not prove which phase is active (or which is most active for FTS); however, it is interesting that the most active catalysts show the weakest signal for Fe_3O_4 and Fe_5C_2 and the strongest signal for Fe_2C.

Figure 8 illustrates the effects of the factorial variables (U/W and H/L) on rate of reaction at 250 °C. The 1W catalysts were excluded to avoid confusion over compounding effects from the lower potassium loadings of these two catalysts. The figure shows higher rates for unwashed catalysts than for washed catalysts. For example, the 2U catalysts show an average 60% increase (14.0 mmol/g/h) in rate compared to 2W catalysts. In addition, for each pair of 1U, 2U, and 2W catalysts, H catalysts show an average 19% increase (5.2 mmol/g/h for 2S catalysts).

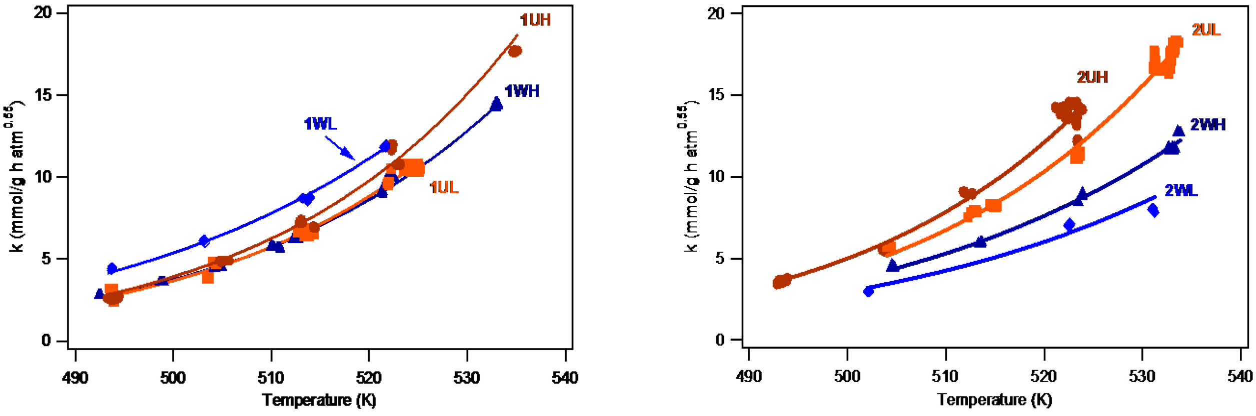

(**a**) (**b**)

Figure 6. Rate constant as a function of temperature for (**a**) 1S and (**b**) 2S catalyst kinetic data sets.

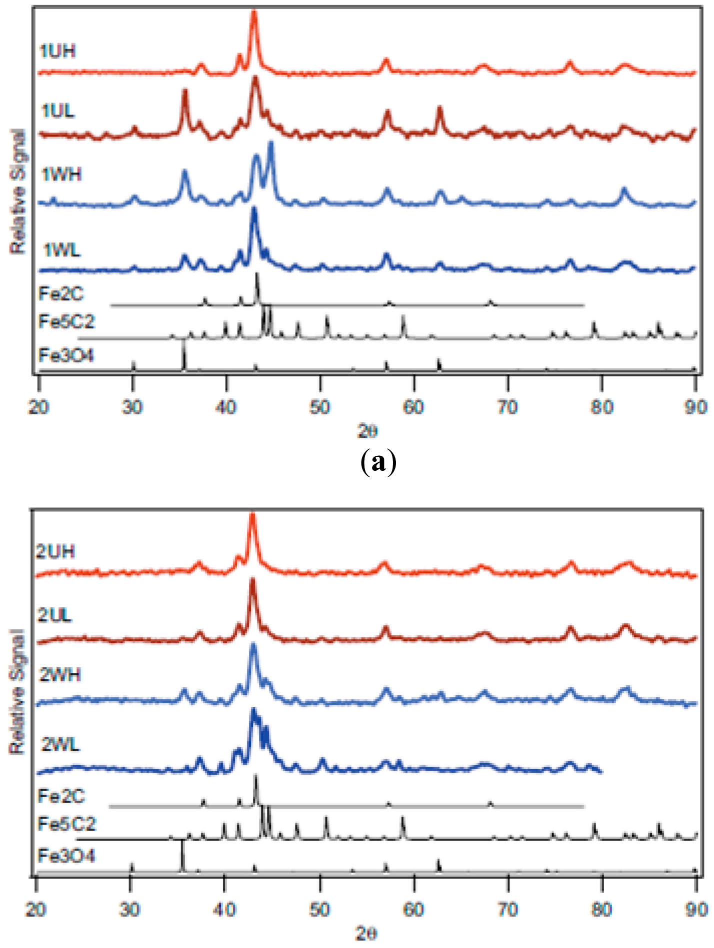

(**a**)

(**b**)

Figure 7. XRD spectra of (**a**) 1S catalysts and (**b**) 2S catalysts after FTS reaction.

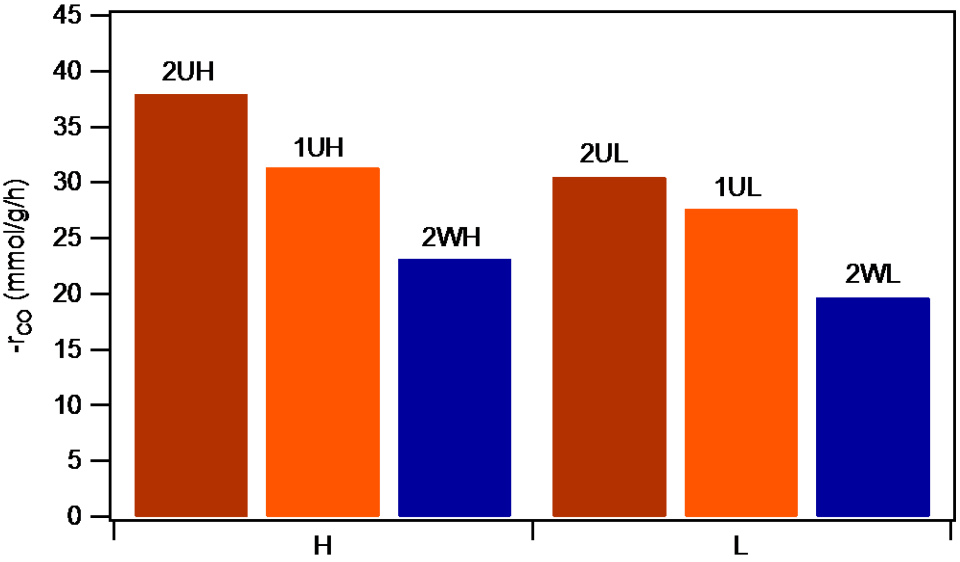

Figure 8. Effects of washing and drying on rate of reaction for 1S and 2S catalysts at 250 °C. 1WH and 1WL are not shown to avoid confusion over effects of low potassium loading.

These activity results indicate that the washing step effects a fundamental change in the nature of the active sites. Site activity is related to binding energy. Sites with low binding energies, like planar sites, can adsorb and desorb reactants quickly and may not allow for sufficient time and contact for the reaction to proceed efficiently. Sites with very high binding energies, like corner sites or defect sites, may bind reactants too strongly and prevent desorption of products. Sites with intermediate binding energies, like edge sites found at the boundaries between crystallites, may provide the majority of the turnover and activity. As discussed in the PSD section, washing removes NH_4NO_3 from between particles and allows them to form larger, more ordered agglomerates as seen in the TEM images of 1WH (Figure 5b). The image of 1WH shows larger, smoother particles than does the image of 1UH (Figure 5a). The surface reorganizations resulting from washing and subsequent grain growth during heat treatments appear to eliminate boundaries between crystallites, resulting in fewer edges and corners therefore eliminating active binding sites and resulting in lower catalyst activities.

Figure 9 shows rate of reaction at 250 °C *versus* crystallite size and pore diameter for 1U and 2S catalysts. 1W catalyst with low K loading are excluded from these charts. It is clear that rate of reaction increases with decreasing particle and pore diameters. U and WH catalysts have particle and pore diameters mainly between 10 and 20 nm which may be ideal for FTS, whereas WL catalysts show larger diameters and lower rates.

2.2.2. Selectivity

For H_2-deficient feed stocks like coal or biomass, the water gas shift (WGS) activity of Fe FT catalysts is important. Table 3 reports the mole percent of CO converted to CO_2 as an indicator of the WGS activity of each catalyst in this study at several temperatures. WGS selectivity increases with increasing temperature for all catalysts in this study. This suggests that the activation energy for the WGS reaction is larger than for the FT reactions.

Table 3. Selectivity of catalysts at different temperatures.

Catalyst	**CO to CH_4 (mole%)** [a,b]			**CO to CO_2 (mole%)** [c]		
	230 °C	240 °C	250 °C	230 °C	240 °C	250 °C
1UH	4.7	5.3	6.3	41.7	43.1	45.2
1UL	4.0	4.6	5.0	38.2	43.3	45.5
1WH	14.8	15.5	15.1	10.7	14.4	18.9
1WL	10.8	12.0	12.5	9.8	14.2	18.0
2UH	6.9	7.2	8.4	30.5	31.2	32.6
2UL	3.6	4.9	6.0	23.2	29.5	34.0
2WH	3.1	3.8	4.9	24.0	28.7	33.9
2WL	5.1	5.5	7.2	31.2	32.5	37.1

[a] CO_2-free basis; [b] 95% confidence interval less than ±0.7%; [c] 95% confidence interval less than ±1.5%.

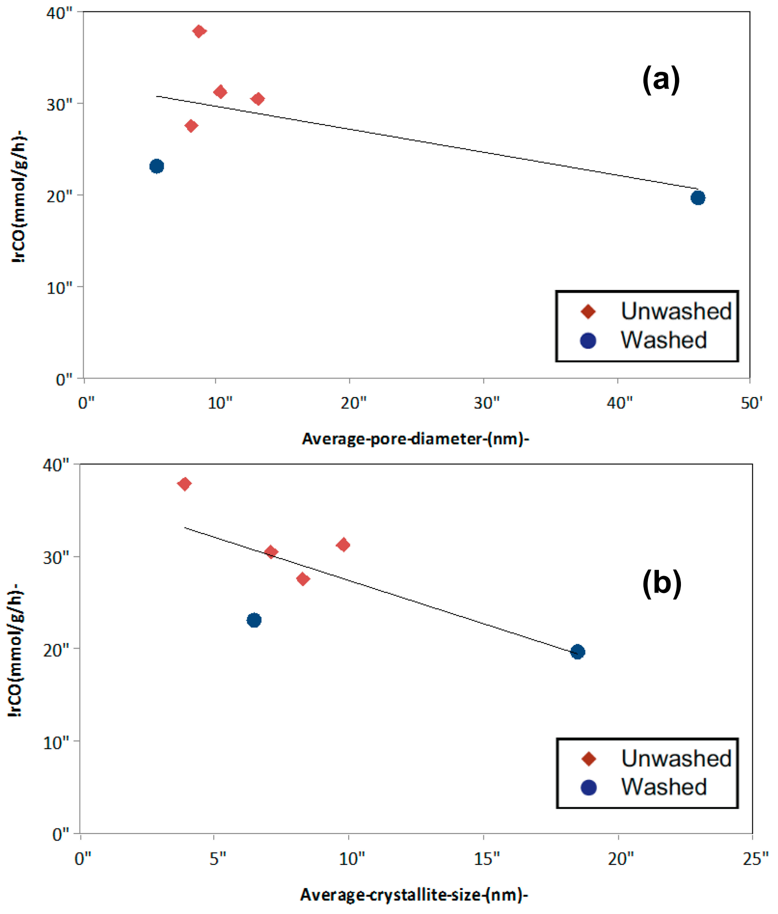

Figure 9. Rate of reaction at 250 °C *versus* (**a**) average crystallite diameter after reduction and (**b**) average pore diameter after passivation.

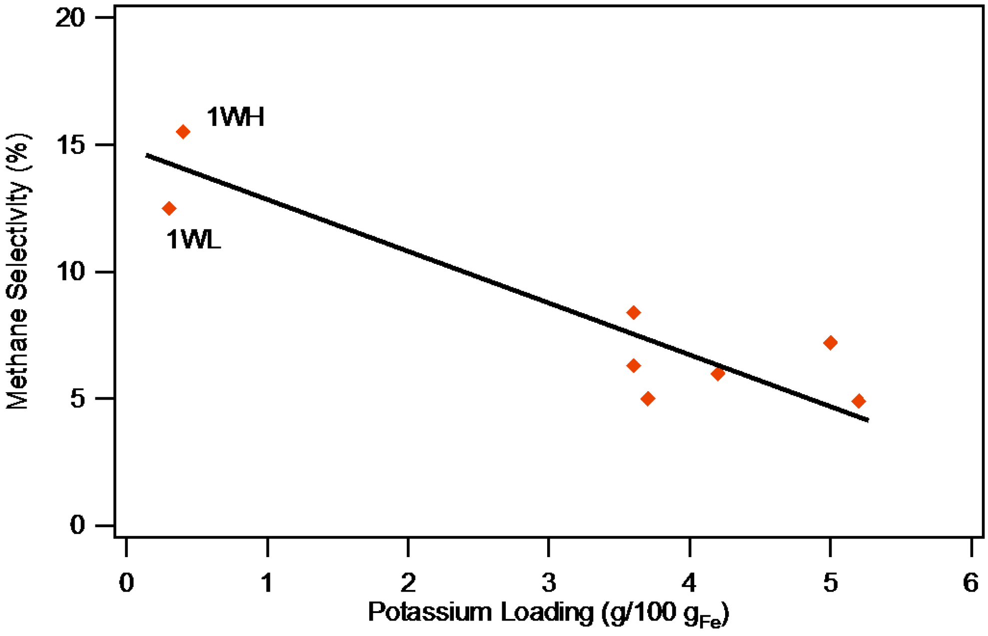

Figure 10. CH_4 selectivity *versus* potassium loading for SDP catalysts.

CH_4 selectivity increases with increasing temperature also, as demonstrated in Table 3. Selectivities for the eight 1S and 2S catalysts appear to increase at about the same rate with temperature suggesting that K loading has little or no effect on the activation energy of the methane reaction. As shown in Figure 10, 1W catalysts (0.3 pbm K) have selectivities 50–200% higher than catalysts with nominal potassium loading (3.6–5.2 pbm K). Decreasing CH_4 selectivity with increasing K loading is well documented in the literature [4,24,29].

The 1U catalysts exhibit the highest WGS activity with 38.2–45.5% selectivity to CO_2. 1W shows the lowest WGS activity of the eight catalysts with 9.8–18.9% selectivity. 2S catalysts fall between these levels. The differences in selectivities may be due to the content and dispersion of K in the catalysts. The higher WGS activities of 1U catalysts may be due to more even distribution and greater dispersion of K, whereas the low WGS activities of the 1W catalysts are probably due to almost complete loss of K during washing (K loadings < 0.4 pbm). The intermediate WGS activities of 2S catalysts reflect K distributions less uniform than 1S catalysts from the microprobe results.

2.2.3 Stability

In addition to activity and selectivity, catalyst stability is a key metric for discerning between catalysts. Both catalyst activity and selectivity can change with time. Figure 11 shows the reaction rate constant for 1UH and 2UH as a function of time-on-stream. As shown in Figure 11a, data of 1UH span more than 500 hours and show little or no downward trend with time, thereby suggesting that this catalyst has excellent activity stability. The variation (scatter) in apparent rate constant measurements may be due in part to inaccurate orders of reaction used to calculate k. In contrast, 2UH shows an apparent constant rate of decrease in activity (deactivation). For illustration purposes, a linear slope and intercept are regressed to the data recorded at 250 °C, excluding the temperature and partial pressure experiments, and are represented by the dark line in Figure 11b. The cause of the deactivation is probably carbon deposition on the catalyst surface where the concentration of K appears to be higher. As shown in microprobe images for promoter distribution (Figure 1), 1S catalysts show more uniform distribution than 2S catalysts. Therefore, in 2S catalysts, the carbon is more likely to deposit on the grain boundaries, where K concentration is higher, and induce catalyst deactivation.

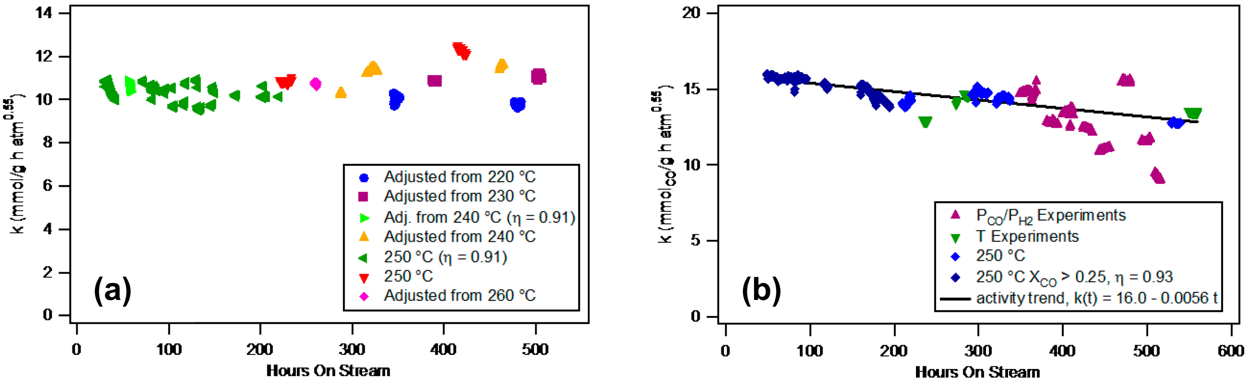

Figure 11. Experimental rate constant values at 250 °C as a function of time-on-stream for (**a**) 1UH and (**b**) 2UH catalysts. Legends represent data converted from different reaction temperatures.

2.2.4 Comparison to Published Catalysts

The catalysts from this study compare well with data on published catalysts in the literature. The activity, productivity, selectivity of 1UH, 2UH, and published, highly active iron catalysts [8] are listed in Table 4. The activity and productivity for 1UH and 2UH are comparable with TAMU catalysts and higher than Mobil catalyst. For the selectivity, although 1UH and 2UH show higher CH_4 selectivity, their C_{2+} selectivity are comparable or even higher than TAMU and Mobil catalysts. While acknowledging that the TAMU catalyst was tested in a slurry phase CSTR, and the Mobil catalyst was tested in a slurry bubble reactor, nevertheless using 1UH and 2UH as proxy, catalysts made by the solvent-deficient precipitation method show great potential for having activity, selectivity, and productivity comparable to those of some of the most active and selective catalysts in the literature. It is important to note that the two published catalysts were subjected to an optimized pretreatment process that significantly enhanced the catalyst activity and productivity. The BYU catalyst pretreatment has not been optimized yet and improvements in catalyst preparation techniques and pretreatment are expected to improve catalytic properties significantly.

Table 4. Comparison of 1UH and 2UH with published, highly active iron catalysts [a].

Catalyst	**Activity (mmol/g h MPa)**	**Productivity (g_{HC}/g_{Fe} h)**	**Selectivity**			
			H_2/CO	**CH_4**	**C_{2+}**	**CO_2**
1UH	125	0.55	1.0	0.040	0.49	0.47
2UH	134	0.71	1.0	0.063	0.61	0.34
TAMU [b]	102-180	0.5-0.8	0.67	0.014	0.50	0.48
Mobil [b]	102	0.39	0.73	0.012	0.49	0.50

[a] Data from ref. [7]; [b] TAMU catalyst operated at 260 °C and 22 atm, Mobil catalyst operated at 257 °C and 15 atm activity in mmol of CO per g Fe per MPa H_2.

3. Experimental Section

3.1 Catalyst Preparation

As illustrated in Scheme 1 and described above, the effects of three key preparation variables—(1) timing of the addition of promoters potassium and silica, (2) presence or absence of a washing step for the precursor, and (3) drying temperature—were investigated by preparing eight catalysts in a 2^3 factorial design. Levels for timing of promoter addition were “1 Step” in which potassium and silica promoters were added to the salts of iron and copper before precipitation,, and “2 Step” in which potassium and silica promoters were added in a separate step after precipitation and washing, if applicable. The levels for washing were unwashed (U) or washed (W) using 100 mL of deionized water five times immediately following precipitation. Levels for initial drying temperature were high (H) temperature (100 °C) and low (L) temperature (60 °C overnight, followed by 100 °C).

The eight catalysts were prepared with target compositions designated as 100 Fe/5 Cu/4 K/16 SiO_2 which indicates relative mass values of each component. In the 1 Step preparation, the silica promoter was added to the iron and copper salts (acid) and the potassium promoter was added to ammonium bicarbonate (base) before combining the two mixtures and stirring vigorously. In a typical preparation, 4.822 g fumed SiO_2 (Cab-O-Sil) were added to 217.005 g $Fe(NO_3)_3 \cdot 9H_2O$ and 5.485g $Cu(NO_3)_2 \cdot 2.5H_2O$ and mixed well with a pestle in a large glass bowl. In a separate container, 3.071 g $KHCO_3$ were mixed with 128.989 g NH_4HCO_3 followed by adding the bicarbonate mixture to the metal salt mixture. The combined mixture of powders was vigorously mixed with the pestle, leading to waters of hydration being released. Mixing continued for approximately 20 min until precipitation of Fe and Cu hydroxides, referred to as the precursor, was complete as indicated by cessation of CO_2 release [15]. Then, the precursor was split into portions which were treated according to their code, respectively, and pelletized, crushed and sieved to −30/+60 mesh. The resulting four catalysts are collectively identified as 1S catalysts.

For the “2 Step” preparations, the Fe and Cu metal salts were precipitated according to the SDP method. The K and Si promoters and enough water to make a thick clay were added to the damp precipitate before drying. For 2UH and 2UL, the promoters were added immediately after complete precipitation and before drying. For 2WH and 2WL, the promoters were added immediately after washing. 2WH was dried at 120 °C instead of 100 °C, but all other precursors were dried at 100 °C for 16–48 hours or at 60 °C for 16–48 hours followed by 100 °C as designated. The dried precursors were pelletized, crushed and sieved to −30/+60 mesh. These catalysts are collectively identified as 2S catalysts.

3.2 Characterization Techniques

3.2.1. N_2 Adsorption

Pore properties were measured by nitrogen adsorption using a Micromeritics TriStar 3000 BET analyzer. Sample sizes were typically 0.3–0.5 g and degassed at 200 °C overnight prior to measurements. Surface areas (SA) were calculated using the BET model using P/P_0 from 0.05 to

0.2 [30]. Pore volume (Vpore) was measured at a single point at P/P_0 of 0.995. Average pore diameter and PSD were calculated using a split pore geometry (SPG) model [31].

3.2.2. Thermal Gravimetric Analysis (TGA)

Temperature programmed oxidation (TPO), temperature programmed reduction (TPR), isothermal oxygen titration and CO chemisorption were performed on 10–40 mg samples in a Mettler Toledo TGA/DSC 1 equipped with an automated GC 200 gas controller. Gas flow rates of H_2, CO, and O_2 (or air depending on the source) were set by rotameters, but gas switching during all experiments was controlled by the GC 200 controller and the TGA software.

TPO experiments were used to design temperature programs for bulk calcination. The rate of mass loss during a constant temperature ramp of 3 °C /min from ambient temperature to 700 °C in 100 mL/min of 70–80% air/He was analyzed to determine appropriate temperature ramps and soaks for controlling byproduct decomposition at low rates.

TPR experiments were used to determine temperature programs for bulk reduction. Again, the rate of mass loss during a straight temperature ramp of 3 °C/min from ambient temperature to 700 °C in 100 mL/min 10% H_2/He was analyzed to determine appropriate temperature ramps and soaks for reduction to proceed at an acceptable rate without producing high partial pressures of H_2O.

Isothermal oxygen titration experiments were used to determine the extent of reduction (EOR) to Fe metal following reduction. EOR was calculated from O_2 uptake during oxidation at 400 °C after the re-reduction of the previously passivated catalyst for 6 hours at 300 °C in 10% H_2/He.

Gravimetric carbon monoxide adsorption was used as a relative measurement of chemisorption site density. CO uptake was measured at 25 °C in 10% CO/He following re-reduction of passivated catalysts at 300 °C for 6 h in 10% H_2/He and a one-hour purge in 100% He at 290 °C.

3.2.3. Hydrogen Chemisorption

Dispersion and crystallite diameters of reduced catalysts were calculated from hydrogen chemisorption uptake measurements. Hydrogen was chemisorbed on reduced catalysts in a flowthrough adsorption system using procedures and equipment developed in the BYU catalysis lab [32]. Passivated catalysts were re-reduced at 300 °C in 100% H_2 for 6 hours followed by purging in Ar at 280 °C to remove residual H_2 from the reduction. Hydrogen was adsorbed at 100 °C before purging at dry ice/acetone temperatures (77 K) to remove physisorbed molecules. Finally, hydrogen was desorbed during a temperature ramp up to 600 °C. Dispersion (*Disp*) and average crystallite diameter (d_c) estimates were calculated from the hydrogen uptake and extent of reduction data using Equations 3 and 4, respectively [2].

$$Disp = 1.12 \times \frac{Hydrogen\ Uptake}{EOR\ \times WeightLoading} \tag{3}$$

$$d_c = \frac{123}{Disp} \tag{4}$$

Crystallite diameter (d_c) is in nm, H_2 uptake is in μmol/g, EOR is the fraction of Fe in the metallic state, and weight loading is the mass percent of Fe in the catalyst.

3.2.4. X-ray Diffraction (XRD)

Crystalline phases of catalysts after drying, calcining, reducing, and carbiding (a result of FB FTS testing) were identified using X-ray diffraction (XRD) patterns in order to understand phase changes at each of these steps and to estimate crystallite diameters. XRD patterns were collected using a PANalytical X'Pert Pro diffractometer with a Cu source and a Ge monochromator tuned to the Cu-Kα1 wavelength (λ = 1.540598 Å). Samples were scanned from 20 to 90° 2θ using a step size of 0.016° at scan rates between 100 and 400 s/step. Diffraction patterns were compared to standard patterns in the International Center for Diffraction Data (ICDD) database. Average crystallite size (d_c) was calculated by Scherrer's formula.

3.2.5 Electron Microscope Analysis

To determine the uniformity of promoter distributions at the micron level, macro elemental distributions of Fe, Cu, K, and Si in 50–400 μm catalyst agglomerates were imaged using a Cameca SX50 electron microprobe at 15 kV and 20–30 nA.

Confirmation of the presence of crystallite diameters estimated from other techniques was attempted with TEM imaging. Crystallites and agglomerates were imaged on a FEI TF30 TEM operating at 300 keV or on a FEI TF20 Ultra-twin TEM/STEM operating at 200 keV.

3.2.6 Inductively Coupled Plasma (ICP) Analysis

To confirm the elemental content of prepared catalysts, digested catalysts and catalyst washes were analyzed in a Perkin Elmer Optima 2000 DV ICP analyzer. Catalyst samples (20–45 mg) were digested in hydrofluoric acid, dried, and then dissolved in 10 mL 3% nitric acid. 0.5–1 mL of digested sample was diluted with 20–40 mL of 3% nitric acid, giving final analyte concentrations of about 100 mg_{cat}/L. Samples of catalyst washes (3–5 mL) were diluted with 15 mL of 3% nitric acid before analysis. Analyte wavelengths were 238.2 nm (Fe), 327.4 nm (Cu), and 766.5 nm (K).

3.3 Activity Tests

Fischer-Tropsch Synthesis (FTS) was conducted in a fixed-bed reactor (stainless steel, 3/8 inch OD) described previously [22,23]. Each sample to be tested (0.25 g, 250–590 μm) was diluted with quartz sand (−50/+70 mesh) to improve temperature stability in the catalytic zone. Before FTS, the sample was reduced *in situ* at 280−320 °C in 10% H_2/He for 10 h followed by 100% H_2 for 6 h. Then, the catalyst was cooled to 180 °C and the system was pressurized to 2.1 MPa in flowing syngas (H_2:CO = 1). The catalyst was then heated (still in syngas) and activated at 280 °C and a CO conversion level of ~60% for 48−90 h. These activation conditions were chosen based on studies by Bukur *et al.* that showed that Fe FTS catalysts activated under syngas had lower deactivation rates compared to those activated under CO and had lower methane selectivity compared to those activated under H_2 [33,34]. After activation, the reactor conditions were changed to those to be tested which included temperatures from 220 °C to 260 °C and H_2:CO ratios from 0.66 to 1.0. In addition to CO and H_2, the feed gas contained 20−40% helium used as a diluent to keep the total pressure the same for all runs. The exit gas and liquid effluent passed through a hot trap (110 °C) and a cold trap (0 °C) to collect heavy hydrocarbons and liquid products. The effluent gaseous product was analyzed using an HP 6890 gas chromatograph equipped with a thermal conductivity detector and 60/80 carboxene-1000 column. CO and H_2 conversions and product selectivities were determined with the aid of an Ar tracer.

The rate of reaction (CO depletion) was determined by operating at low CO conversions ($X_{co} \leq 0.25$), assuming differential reactor conditions, and thus using the resulting reactor performance equation:

$$-r_{co} = \frac{F_{co}^{0} X_{co}}{W_{cat}} \tag{5}$$

where W_{cat} is the mass of catalyst and $F_{CO}{}^{0}$ is the inlet molar CO flow rate. Experimental rate constant (k) values were determined for every data point from the rate data using Equation 6 by assuming the P_{CO} and P_{H2} dependencies proposed by Eliason [35]. Values of P_{H2} and P_{CO} are simple averages of the inlet and outlet partial pressures of each gas.

$$k = \frac{-r_{co}}{P_{CO}^{-0.05} P_{H_2}^{0.6}} \tag{6}$$

4. Conclusions

In summary, we have successfully prepared active and stable iron FT catalysts via a facile, solvent-deficient precipitation method. Key preparation variables, *i.e.*, drying, washing, and promoter addition step, were identified by a 2^3 factorial experimental design. Results in this study show that (1) unwashed catalysts are statistically more active (60% on average) than washed catalysts of the same potassium loading; (2) catalysts dried initially at higher temperature (100 °C) are more active (~20%) than catalysts dried initially at lower temperature (60 °C); (3) 1S (one-step preparation) catalysts appear to have superior properties to 2S catalysts under reaction conditions when considering activity, selectivity, and stability together; (4) catalysts with average particle diameters and average pore sizes both between 5 and 15 nm are up to 300% more active than catalysts with larger average particle (17–23 nm) and pore diameters (45–50 nm). In addition, 1UH and 2UH in this study show comparable or even better activity, selectivity, and stability than those of published, highly active catalysts, though consideration should be given to the different reactor geometries used in the various catalyst tests. As a simple and time-effective method, solvent-deficient precipitation not only contributes to the development of iron FT catalysts, but also offers promising potential for preparation of other catalysts used in different applications.

Acknowledgements

We thank Jeff Farrer and BYU microscopy lab for their assistance with TEM imaging. The financial support for this work was provided by members of the Brigham Young University Fischer-Tropsch Consortium and the University of Wyoming Clean Coal Technologies program.

Author Contributions

Kyle M. Brunner prepared the catalysts, performed the experiments and wrote the original manuscript. Baiyu Huang helped prepare the final manuscript. William C. Hecker supported the catalyst preparation, the experiments and revised the final version of paper. Brian F. Woodfield was instrumental in the development of the SDP method.

Conflicts of Interest

The authors declare no conflict of interest.

References

1. Schulz, H. In *Fischer-Tropsch Synthesis in a Modern Perspective*; Wiley-VCH Verlag GmbH & Co. KGaA: WeinHeim, Germany 2012; pp. 301–324.
2. Bartholomew, C.H.; Farrauto, R.J. *Fundamentals of Industrial Catalytic Processes*; Wiley: Hoboken, U.S.A 2011.
3. Steynberg, A.P. Introduction to Fischer-Tropsch technology. *Fischer-Tropsch Technol.* **2004**, *152*, 1–63.
4. Dry, M.E. Chapter 4 In *The Fischer-Tropsch Synthesis*; Springer: Berlin, Germany 1981; pp. 159–255.
5. Bukur, D.B.; Lang, X.; Mukesh, D.; Zimmerman, W.H.; Rosynek, M.P.; Li, C.P. Binder Support Effects on the Activity and Selectivity of Iron Catalysts in the Fischer-Tropsch Synthesis. *Ind. Eng. Chem. Res.* **1990**, *29*, 1588–1599.
6. Bukur, D.B.; Koranne, M.; Lang, X.S.; Roa, K.R.P.M.; Huffman, G.P. Pretreatment Effect Studies with a Precipitated Iron Fischer-Tropsch Catalyst. *Appl. Catal. A* **1995,** *126*, 85–113.
7. Bukur, D.B.; Lang, X.S. A precipitated iron Fischer-Tropsch catalyst for synthesis gas conversion to liquid fuels. *Natural Gas Convers. V* **1998**, *119*, 113–118.
8. Bukur, D.B.; Lang, X.S. Highly active and stable iron Fischer-Tropsch catalyst for synthesis gas conversion to liquid fuels. *Ind. Eng. Chem. Res.* **1999**, *38*, 3270–3275.
9. Li, S.Z.; Krishnamoorthy, S.; Li, A.W.; Meitzner, G.D.; Iglesia, E., Promoted iron-based catalysts for the Fischer-Tropsch synthesis: Design, synthesis, site densities, and catalytic properties. *J. Catal.* **2002**, *206*, 202–217.
10. Wu, B.; Bai, L.; Xiang, H.; Li, Y.-W.; Zhang, Z.; Zhong, B. An active iron catalyst containing sulfur for Fischer–Tropsch synthesis. *Fuel* **2004**, *83*, 205–212.
11. Yang, Y.; Xiang, H.W.; Zhang, R.L.; Zhong, B.; Li, Y.W. A highly active and stable Fe-Mn catalyst for slurry Fischer-Tropsch synthesis. *Catal. Today* **2005**, *106*, 170–175.
12. Ma, W.; Jacobs, G.; Graham, U.M.; Davis, B.H. Fischer-Tropsch Synthesis: Effect of K Loading on the Water-Gas Shift Reaction and Liquid Hydrocarbon Formation Rate over Precipitated Iron Catalysts. *Top. Catal.* **2014**, *57*, 561–571.
13. Park, J.-Y.; Lee, Y.-J.; Jun, K.-W.; Bae, J.W.; Viswanadham, N.; Kim, Y.H. Direct conversion of synthesis gas to light olefins using dual bed reactor. *J. Ind. Eng. Chem.* **2009,** *15*, 847–853.
14. Liu, S.F.; Liu, Q.Y.; Boerio-Goates, J.; Woodfield, B.F. Preparation of a wide array of ultra-high purity metals, metal oxides, and mixed metal oxides with uniform particle sizes from 1 nm to bulk. *J. Adv. Mater.* **2007**, *39*, 18–23.
15. Bartholomew, C.H.; Woodfield, B.F.; Huang, B.; Olsen, R.E.; Astle, L. Method for making highly porous, stable metal oxide with a controlled pore structure. WO2011119638A2, March 2011.

16. Huang, B.; Bartholomew, C.H.; Smith, S.J.; Woodfield, B.F. Facile solvent-deficient synthesis of mesoporous γ-alumina with controlled pore structures. *Microporous Mesoporous Mater.* **2013**, *165*, 70–78.
17. Huang, B.; Bartholomew, C.H.; Woodfield, B.F., Facile structure-controlled synthesis of mesoporous γ-alumina: Effects of alcohols in precursor formation and calcination. *Microporous Mesoporous Mater.* **2013**, *177*, 37–46.
18. Huang, B.; Bartholomew, C.H.; Woodfield, B.F., Facile synthesis of mesoporous γ-alumina with tunable pore size: The effects of water to aluminum molar ratio in hydrolysis of aluminum alkoxides. *Microporous Mesoporous Mater.* **2014**, *183*, 37–47.
19. Khosravi Mardkhe, M.; Woodfield, B.; Bartholomew, C. Facile one-pot synthesis of a thermally stable silica-doped alumina having a large pore volume and large bimodal pores. In Proceedings of 247th ACS National Meeting, Dallas, TX, USA, 16–20 March 2014.
20. Olsen, R.E.; Bartholomew, C.H.; Huang, B.Y.; Simmons, C.; Woodfield, B.F. Synthesis and characterization of pure and stabilized mesoporous anatase titanias. *Microporous Mesoporous Mater.* **2014**, *184*, 7–14.
21. Smith, S.J.; Page, K.; Kim, H.; Campbell, B.J.; Boerio-Goates, J.; Woodfield, B.F. Novel synthesis and structural analysis of ferrihydrite. *Inorg. Chem.* **2012**, *51*, 6421–6424.
22. Brunner, K.M.; Harper, G.E.; Keyvanloo, K.; Woodfield, B.F.; Bartholomew, C.H.; Hecker, W.C. Preparation of Unsupported Iron Fischer-Tropsch Catalyst by Simple, Novel, Solvent Deficient Precipitation (SDP) Method. *Energy Fuels* **2015**, *29*, 1972–1977.
23. Brunner, K.M. Novel Iron Catalyst and Fixed-Bed Reactor Model for the Fischer-Tropsch Synthesis. Ph.D. Thesis, Brigham Young University, August 2012.
24. Bukur, D.B.; Mukesh, D.; Patel, S.A.; Rosynek, M.P.; Zimmerman, W.H. Development and Process Evaluation of Improved Fischer-Tropsch Slurry Catalysts. Available online: http://www.fischer-tropsch.org/DOE/DOE_reports/80011/80011-1/80011-1_toc.htm (accessed on 23 July 2015).
25. Ristić, M.; De Grave, E.; Musić, S.; Popović, S.; Orehovec, Z., Transformation of low crystalline ferrihydrite to α-Fe_2O_3 in the solid state. *J. Mol. Struct.* **2007**, *834–836*, 454–460.
26. Feng, Z.; Zhao, J.; Huggins, F.E.; Huffman, G.P. Agglomeration and Phase-Transition of a Nanophase Iron-Oxide Catalyst. *J. Catal.* **1993**, *143*, 510–519.
27. Eggleton, R.A.; Fitzpatrick, R.W. New Data and a Revised Structural Model for Ferrihydrite. *Clays Clay Miner.* **1988**, *36*, 111–124.
28. Zhao, J.M.; Huggins, F.E.; Feng, Z.; Huffman, G.P., Ferrihydrite - Surface-Structure and Its Effects on Phase-Transformation. *Clays Clay Miner.* **1994**, *42*, 737–746.
29. Arakawa, H.; Bell, A.T., Effects of Potassium Promotion on the Activity and Selectivity of Iron Fischer-Tropsch Catalysts. *Ind. Eng. Chem. Process Des. Dev.* **1983**, *22*, 97–103.
30. Gregg, S.J.; Sing, K.S.W. *Adsorption, Surface Area, and Porosity*; Academic Press: San Diego, USA, 1991.
31. Huang, B.; Bartholomew, C.H.; Woodfield, B.F., Improved calculations of pore size distribution for relatively large, irregular slit-shaped mesopore structure. *Microporous Mesoporous Mater.* **2014**, *184*, 112–121.
32. Jones, R.D.; Bartholomew, C.H., Improved Flow Technique for Measurement of Hydrogen Chemisorption on Metal-Catalysts. *Appl. Catal.* **1988**, *39*, 77–88.

33. Bukur, D.B.; Nowicki, Z.; Manne, R.K.; Lang, X. Activation studies with a precipitated iron catalysts for Fischer-Tropsch synthesis. II. Reaction studies. *J. Catal.* **1995**, *155*, 366–375.
34. Bukur, D.B.; Okabe, K.; Rosynek, M.P.; Li, C.; Wang, D.; Rao, K.R.P.M.; Huffman, G.P. Activation studies with a precipitated iron catalyst for Fischer-Tropsch synthesis. I. Characterization studies. *J. Catal.* **1995**, *155*, 353–365.
35. Eliason, S.A. Bartholomew, C.H., Kinetics and Deactivation of Unpromoted and Potassium-Promoted Iron Fischer-Tropsch Catalysts at Low Pressure (1 Atm). *Stud. Surf. Sci. Catal.* **1991**, *68*, 211–218